RESEARCH ARTICLE

INTERNATIONAL RESEARCH JOURNAL OF MULTIDISCIPLINARY TECHNOVATION

Asian Research Association

DOI: 10.54392/irjmt25322

Integration of Modified Luo Converter and ANFIS MPPT in Grid-Tied Photovoltaic Systems

D. Thivya Prasad [a, *], R. Anandhakumar [a], P. Balamurugan [b]

[a] Department of Electrical and Electronics Engineering, Faculty of Engineering and Technology, Annamalai University, Chidambaram, Tamil Nadu, India.

[b] Department of of Electrical and Electronics Engineering, Mount Zion College of Engineering and Technology, Pudukkottai, India.

* Corresponding Author Email: dthivyaprasad45@gmail.com

DOI: https://doi.org/10.54392/irjmt25322

Received: 21-12-2024; Revised: 14-05-2025; Accepted: 23-05-2025; Published: 26-05-2025

Abstract: The sustainable growth of energy solutions depends on the incorporation of renewable energy sources into grid connected systems. This study describes a grid tied photovoltaic (PV) system that uses a modified Luo converter and Maximum Power Point Tracking (MPPT) based on an Adaptive Neuro Fuzzy Inference System (ANFIS). The proposed system integrates a Modified Luo Converter for efficient DC-DC conversion, ensuring stable voltage regulation under varying solar irradiance and temperature conditions. It utilizes an ANFIS based MPPT controller to optimize energy extraction by accurately tracking the PV array's maximum power point, while an LC filter ensures high quality power delivered to the grid in compliance with grid standards. The developed research, executed utilizing MATLAB 2021a Simulink tool, demonstrates exceptional performance with an efficiency of 94.1% and enhanced grid stability.

Keywords: Grid tied PV system, Modified Luo converter, ANFIS, MPPT, DC-DC conversion, PI controller.

1. Introduction

The growing economic development and energy demand have led to widespread adoption of PV systems in industry, offering key advantage being a cleaner and more environmentally friendly alternative to conventional power generation [1]. Among these, PV systems emerged as a reliable and sustainable solution for clean energy generation [2, 3]. Grid tied PV systems, which directly connect solar power to the utility grid, gained significant attention for their potential to enhance energy efficiency and reduce dependence on conventional power sources [4, 5].The growing global energy demand and environmental concerns intensified the focus on renewable energy sources, particularly PV systems, as sustainable and environmental friendly solution [6]. Grid-tied PV systems are crucial for integrating solar energy into existing power grids. [7, 8]. However, ensuring efficient energy conversion and reliable grid interaction remains a significant challenge due to the intermittency and nonlinear characteristics of solar energy [9]. Conventional energy conversion and MPPT methods in PV systems often struggle to maintain efficiency under fluctuating irradiance and temperature conditions. [10, 11].

Traditional DC-DC converters, such as the CUK and Flyback converters, are commonly used for power conditioning in PV systems. The CUK converter is ideal for medium to low power applications with flexible voltage conversion and low ripple, making it suitable for battery charging and sensitive loads, but its complexity, size, cost and higher switching losses limit its use in high power applications [12, 13]. Further, Flyback converter is compact and provides galvanic isolation, making it suitable for off grid PV systems. However, its lower efficiency and limited scalability make it less appropriate for large scale systems [14]. Similarly, MPPT algorithms, Perturb and Observe (P&O) method is simple and cost effective, ideal for stable conditions. Though, it struggles with oscillations, slow response to rapid changes, and sensitive to noise, making it less effective under fluctuating irradiance [15]. In contrast, the Incremental Conductance (INC) algorithm offers accurate and fast MPP tracking, minimizing oscillations and well handling of noise, particularly in dynamic conditions. Due to its complexity, higher computational load and need for additional sensors increase power consumption, making it less suitable for resource limited systems [16].

To address these challenges, this paper proposes an integrated system combining a modified Luo converter with ANFIS based MPPT for grid tied PV applications. The modified Luo converter with its superior voltage gain and efficiency, ensures stable DC power delivery to the grid interface. Meanwhile, The ANFIS MPPT algorithm combines neural networks and

fuzzy logic for accurate, adaptive tracking of the maximum power point, even in complex environmental conditions. This proposed system enhances the energy harvesting efficiency, minimizes power losses and ensures smooth grid interaction, thereby overcoming the limitations of existing technologies.

2. Proposed System Description

To improve energy conversion efficiency and guarantee steady power delivery to the grid, a modified Luo converter is integrated with an ANFIS based MPPT controller in grid PV system. The first component of the system is a PV array, which generates PV voltage and current by converting sunlight into electrical energy. The Pulse Width Modulation (PWM) generator receives optimal control signals from the ANFIS MPPT controller, which dynamically monitors the PV system's maximum power point under changing temperature and sunlight circumstances. The Modified Luo Converter is a high efficiency converter increases the output voltage of PV for grid integration is controlled by these signals, as seen in Figure. 1.

The processed DC voltage is then fed into a Single Phase Voltage Source Inverter (VSI) that converts it into an AC voltage compatible with grid standards. The inverter's operation is managed by another PWM generator, driven by PI controller. This controller regulates reactive and active power delivered into grid by comparing the reference power values with actual values and minimizing errors. An LC filter further smoothes the AC waveform to reduce harmonic distortions, ensuring compliance with grid requirements. This integrated system achieves optimal energy harvesting, efficient power conversion and reliable grid-tied operation, making it a robust solution for solar energy systems.

3. Proposed System Modelling

3.1 PV Cell model

A PV cell converts photon energy into electrical power. To produce clean, green energy, various PV cells coupled in parallel or series serve as PV module. The addition of series (R_s) and shunt (R_{sh}) resistances, which stand in for the intrinsic resistance of cell, makes the solar cell's equivalent circuit, illustrated in Figure 2.

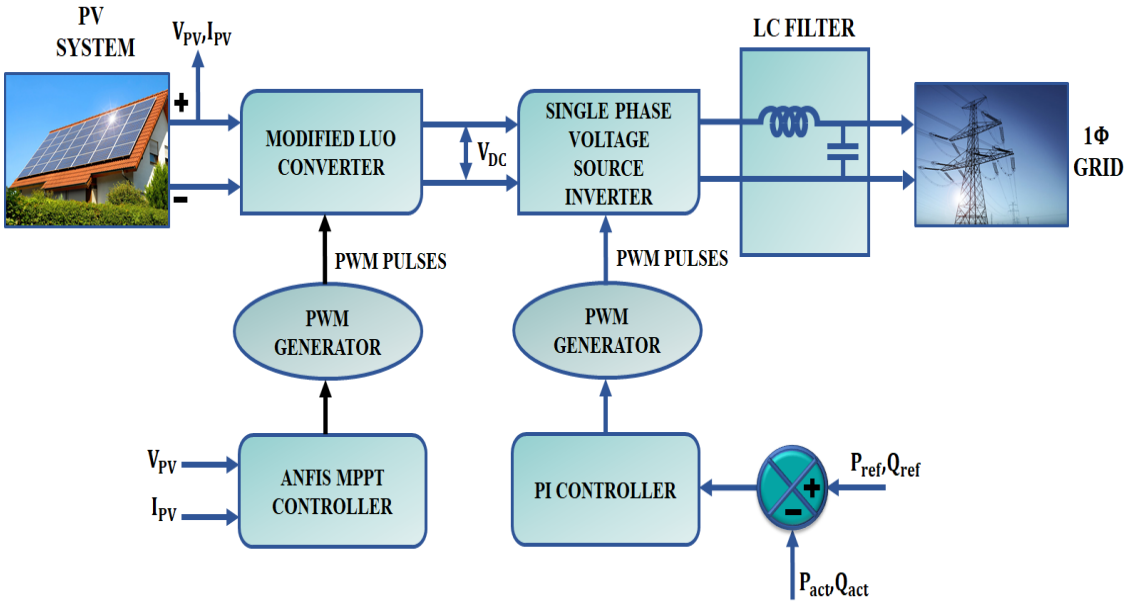

Figure 1. Proposed block diagram of PV system

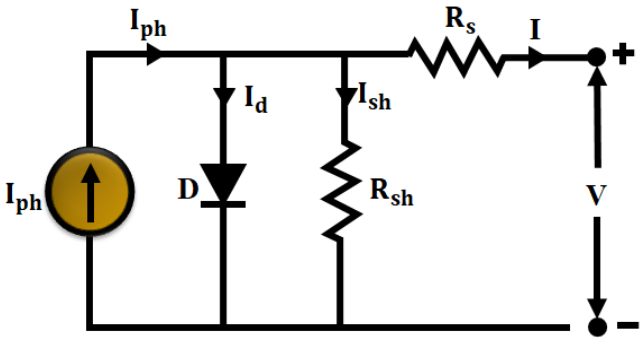

Figure 2. Circuit diagram of PV system

The PV cell's real equivalent circuit output current is provided by equation 1.

$$I = I_{ph} - I_d - I_{sh} \quad (1)$$

The shunt current (I_{sh}), is determined by the circuit using equation 2.

$$I_{sh} = \left(\frac{V+IR_s}{R_{sh}}\right) \quad (2)$$

Both R_s and R_{sh} are measured in ohms. The voltage across the diode is,

$$V_d = V + IR_s \quad (3)$$

$$V_T = \frac{\eta KTN_s}{q} \quad (4)$$

$$I = I_{ph} - I_0\left[exp\left(\frac{q\times(V+IR_s)}{\eta KTN_s}\right) - 1\right] - I_{sh} \quad (5)$$

Where, the number of cells linked in series is N_s, q is the charge of an electron C, k is Boltzmann's constant, and η is the diode's ideality factor, the solar cell's final output current is denoted by I. Due to the low voltage of PV panels, Modified Luo converter is used to boost the voltage.

3.2 Modified Luo Converter

The proposed topology's circuit diagram, displayed in Figure 3, is made up of a series of boost and Luo converters. For applications involving renewable energy. Constant input current is ensured by the exploitation of boost converter in first stage. This configuration reduces the size of input filter capacitor as well as the strain on its current. Within Continuous Conduction Mode (CCM), the converter functions in two modes. For the analysis, it is assumed that the components operate ideally and the steady state conditions are used to define the converter's performance in CCM include a sufficiently large amount for the capacitor voltage to remain constant.

Mode 1

When switch begins to conduct in working, diodes $D_1 and\ D_3$ become forward biased and engaged. As a result, the inductors' voltages are increased and they become magnetic. The negative current causes the converter's first and output capacitors to discharge, while the positive current charges the second capacitor. Figure 4 displays the proposed converter's circuit diagram in this mode. Switch stays in the second operating mode, while the diodes $D_1 and\ D_3$ are reverse biased, which essentially stops current from passing through them.

Mode 2

In the second operation mode, the diodes $D_2 and\ D_4$ begin to conduct, allowing current to pass through them. The converter's circuit diagram in this mode is displayed in fig 5. The inductors demagnetize when the applied voltage drops to a negative value. The charging process of the first and output capacitors is thus started when the currents flowing through them turn positive. The capacitor current and inductor voltage are expressed by ,

$$\begin{cases} L_1\frac{di_{L_1}}{dt} = V_{in}D + (v_{in} - v_{c_1})(1-D), L_2\frac{di_{L_2}}{dt} = v_{c_1}D + (2v_{c_1} - v_0)(1-D) \\ C_1\frac{dv_{c_1}}{dt} = -(i_{L_1} + i_{c_2})D + (i_{L_1} + i_{L_2})(1-D), C_1\frac{dv_{c2}}{dt} = i_{c_2}D - i_{L_2}(1-D) \\ C_0\frac{dv_{c_0}}{dt} = -i_0D + (i_{L_2} + i_0)(1-D) \end{cases} \quad (6)$$

Both the average inductor voltage and capacitor current fall to 0 when the second balancing for inductor voltage and capacitor current is applied. The average inductor current and current and voltage of capacitor are represented by the following formulas:

$$\begin{cases} V_{c1} = \frac{V_{in}}{(1-D)}, \\ IL_1 = \frac{(2-D)}{(1-D)^2}I_0, IL_2 = \frac{1}{1-D}I_0 \end{cases} V_{c2} = \frac{V_{in}}{(1-D)}, V_{c0} = \frac{(2-D)v_{in}}{(1-D)^2} \quad (7)$$

The switches and diodes are stressed by inductor currents when semiconductors are active, whereas the capacitor voltage causes voltage stress when the semiconductors are inactive. The input voltage, output current and duty cycle all show how stressed the semiconductors are by voltage and current.

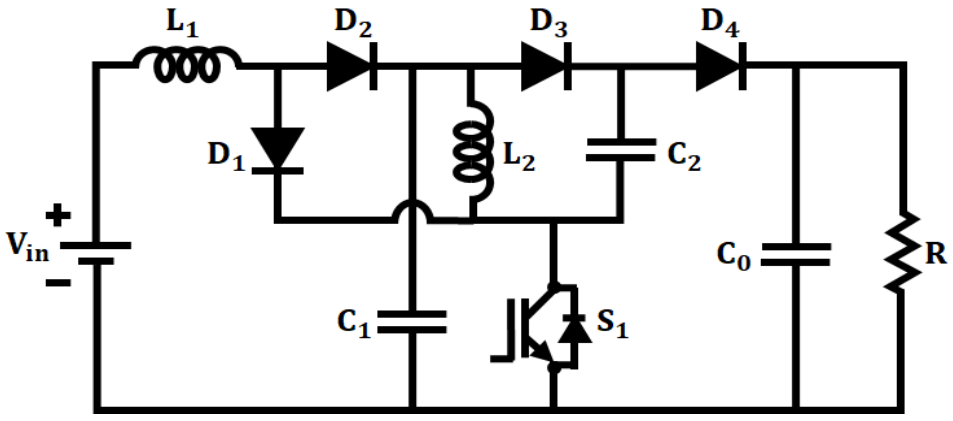

Figure 3. The proposed topology

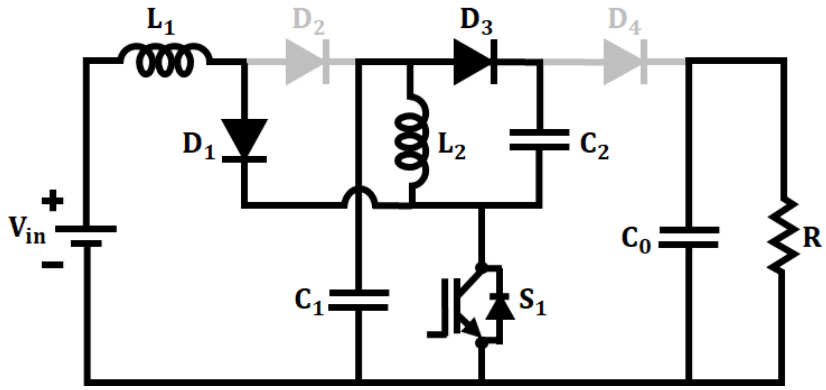

Figure 4. Circuit of the mode 1

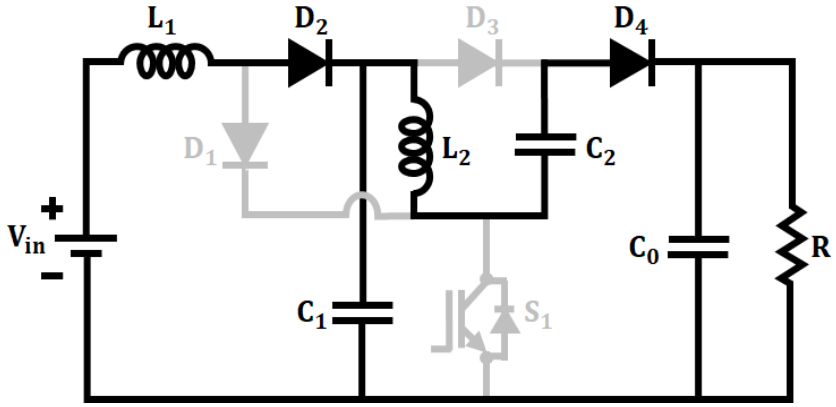

Figure 5. Circuit of the mode 2

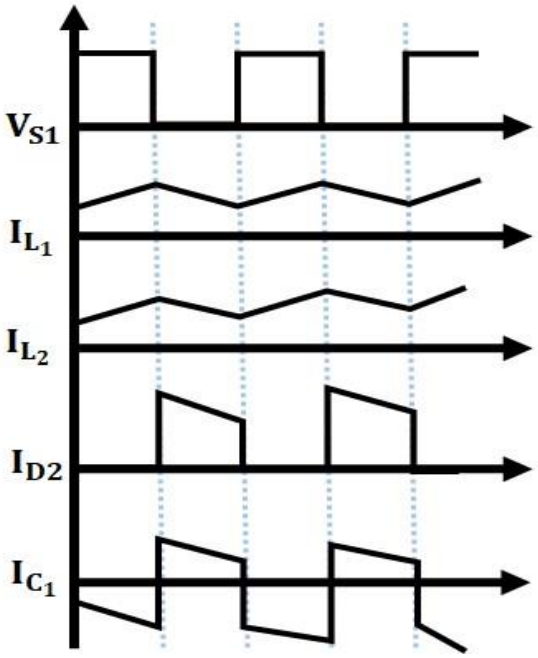

Figure 6. Waveform of the modified Luo converter

$$\begin{cases} I_{S_1} = \frac{(1+D-D^2)I_0}{(1-D)^2},\ I_{D_1} = \frac{D(2-D)I_0}{(1-D)^2}, I_{D_2} = \frac{(2-D)I_0}{(1-D)}, I_{D_3} = I_{D_4} = I_0 \\ V_{S_1} = V_{D_3} = V_{D_4} = \frac{V_{in}}{(1-D)^2}, V_{D_1} = \frac{DV_{in}}{(1-D)^2}, V_{D_2} = \frac{V_{in}}{(1-D)}, \end{cases} \quad (8)$$

Inductor current ripple is the difference among the minimum and maximum inductor currents, while inductor voltage plays a simpler role in operation. Capacitor voltage ripple is the difference between the highest and lowest capacitor voltages and capacitor current decreases during operation. The ripples in

capacitor voltage and inductor current are expressed as follows:

$$\Delta i_{L_1} = \frac{DV_{in}}{L_1 f_s}, \Delta i_{L_2} = \frac{DV_{in}}{(1-D)L_2 f_s}, \Delta v_{c_1} = \frac{DV_0}{(1-D)RC_1 f_s}, \Delta v_{c2} = \frac{V_0}{RC_2 f_s}, \Delta v_{c0} = \frac{DV_0}{C_0 f_s} \quad (9)$$

In mode 1,

$$V_{L1(ON)} = V_{in} \quad (10)$$

In mode 2,

$$V_{L1(OFF)} = V_{in} - V_{C1} \quad (11)$$

By applying voltage-second balance law,

$$V_{in}\, D + (V_{in} - V_{C1}).(1 - D) = 0 \quad (12)$$

$$V_{in}\, D + V_{in}\,(1 - D) - V_{C1}(1 - D) = 0 \quad (13)$$

$$V_{in} - V_{C1}(1 - D) = 0 \quad (14)$$

For inductor L_2,

In mode 1,

$$V_{L2(ON)} = V_{C1} \quad (15)$$

$$V_{L2(OFF)} = 2V_{C1} - V_0 \quad (16)$$

By applying voltage-second balance law,

$$V_{C1}.D + (2V_{C1} - V_0).(1 - D) = 0 \quad (17)$$

$$V_{C1}.D + 2V_{C1}.(1 - D) - V_0(1 - D) = 0 \quad (18)$$

$$V_{C1}(D + 2 - 2D) = V_0(1 - D) \quad (19)$$

$$V_{C1}(2 - D) = V_0(1 - D) \quad (20)$$

$$V_0 = V_{C1}.\frac{2-D}{1-D} \quad (21)$$

$$V_0 = \frac{V_{in}}{1-D}.\frac{2-D}{1-D} \quad (22)$$

$$V_0 = V_{in}.\frac{2-D}{(1-D)^2} \quad (23)$$

The voltage gain is,

$$\frac{V_0}{V_{in}} = \frac{2-D}{(1-D)^2} \quad (24)$$

For duty cycle $(D = 0.6)$, $\frac{V_0}{V_{in}} \simeq 10$ (25)

Ripple expressions underscore the converter's reliance on duty cycle, switching frequency and component values, highlighting the need for optimized design to ensure efficient and stable operation.

3.3 ANFIS based MPPT controller

Integrating the fuzzy logic and neural networks, the ANFIS controller provides MPPT with high tracking accuracy and quick convergence. It generates fuzzy inference rules to adjust membership functions, minimizing error and achieving optimal performance. By iteratively refining these functions, the system learns and adapts, while training data is used to correct any errors and improves accuracy.

Rule 1: $f_1 = P_1x + q_1y + r_1$ if x is A_1 and y is B_1

Rule 2: $f_2 = P_2x + q_2y + r_2$ if x is A_2 and y is B_2

In an ANFIS, x and y are inputs, while A_i and B_i represents fuzzy variables. The outputs, f_i are part of fuzzy sets and the design parameters, p_iq_i and r_i are established during the training phase. The ANFIS architecture in Fig. 7 comprises 5 layers with circles representing fixed nodes and squares for adaptive nodes. Each layer performs specific functions, as detailed below.

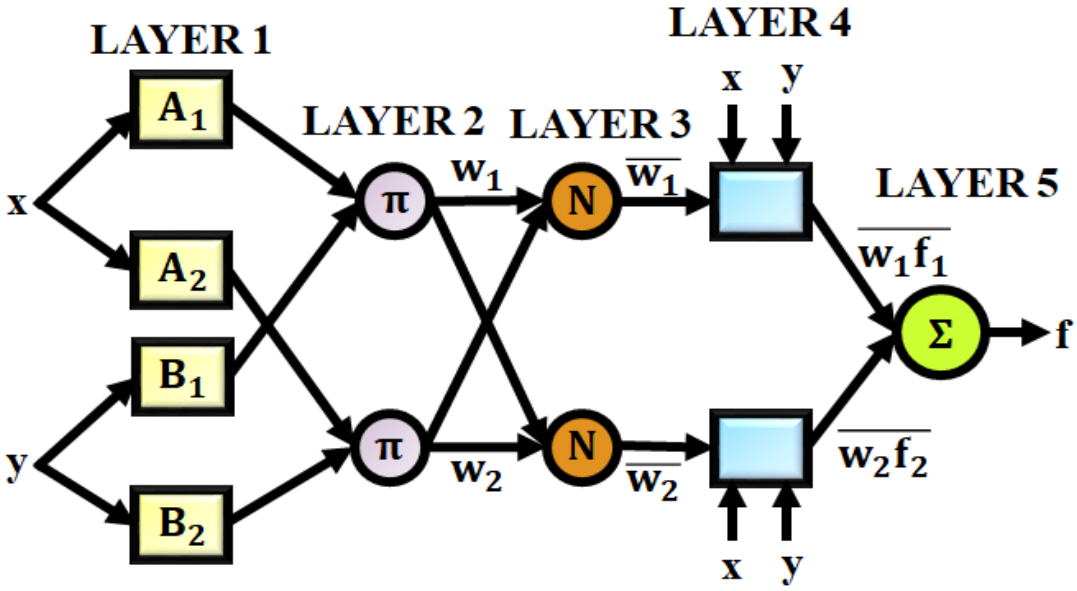

Figure 7. ANFIS based MPPT algorithm

Layer 1

The fuzzy membership grades of inputs, layer 1 outputs are,

$$O_{1,i} = \mu_{A_i}(x), \qquad i = 1,2 \tag{26}$$

$$O_{1,i} = \mu_{B_{i-2}}(y), \qquad i = 3 \tag{27}$$

Here x and y are the inputs to node i in this system, while A_i and B_i are linguistic labels (such as high or low) connected to the functions of the node. Any fuzzy membership used with the membership functions $\mu_{Ai}(x)$ and $(\mu_{Bi-2}(y))$. For instance, $\mu_{Ai}(x)$ is defined appropriately if a bell shaped membership function is employed.

$$\mu_{Ai} = \frac{1}{1+\left[\left(\frac{x-c_i}{a_i}\right)\right]b_i}, \qquad i = 1,2 \tag{28}$$

Where the membership function's parameters are $a_i, b_i, and\ c_i$

Layer 2

Layer 2 nodes are fixed, using the AND operator to fuzzyfy inputs with a basic multiplier function, denoted by π. The output of this layer is,

$$O_2, i = w_i = \mu_{A_i}(x) * \mu_{B_i}(y), \qquad i = 1,2 \tag{29}$$

These are the rules' known firing strengths.

Layer 3

Similar to fixed nodes in layer 3 are indicated by N, signifying their function of normalizing the firing strengths from the layer above. The output of this layer is shown by,

$$O_3, i = \overline{w_i} = \frac{w_i}{w_1+w_2}, \qquad i = 1,2 \tag{30}$$

The results of this layer are called normalized firing strengths.

Layer 4

The adaptive nodes in Layer 4 outputs is the product of normalized firing strength and a first order polynomial in a Sugeno model. The following is how the output is expressed:

$$O_4, i = \overline{w_i} f_i = \overline{w_i(p_i x + q_i y + r_1)}, \qquad \iota - 1,2 \tag{31}$$

Where $p_i, q, and\ r_i$ the ensuing parameters and $\overline{w}$ are the layer 3 output.

Layer 5

The fixed node with the label "x" exists in layer 5. All incoming signals are added by this node labeled with $\sum x$. The model's overall output is provided by,

$$O_5, i = \sum_i \overline{w} f_i = \frac{\sum_i w_i f_i}{\sum_i w_i} \tag{32}$$

The final output represents the optimal MPPT value, which is obtained as the weighted average of the fuzzy rule outputs, enabling the system to track maximum power point while minimizing error through adaptive learning of membership functions.

3.4 Grid voltage synchronization

Grid tied PV system to maximize generation of energy, sustain power quality, comply with grid codes and assure safety, grid voltage synchronization is necessary.

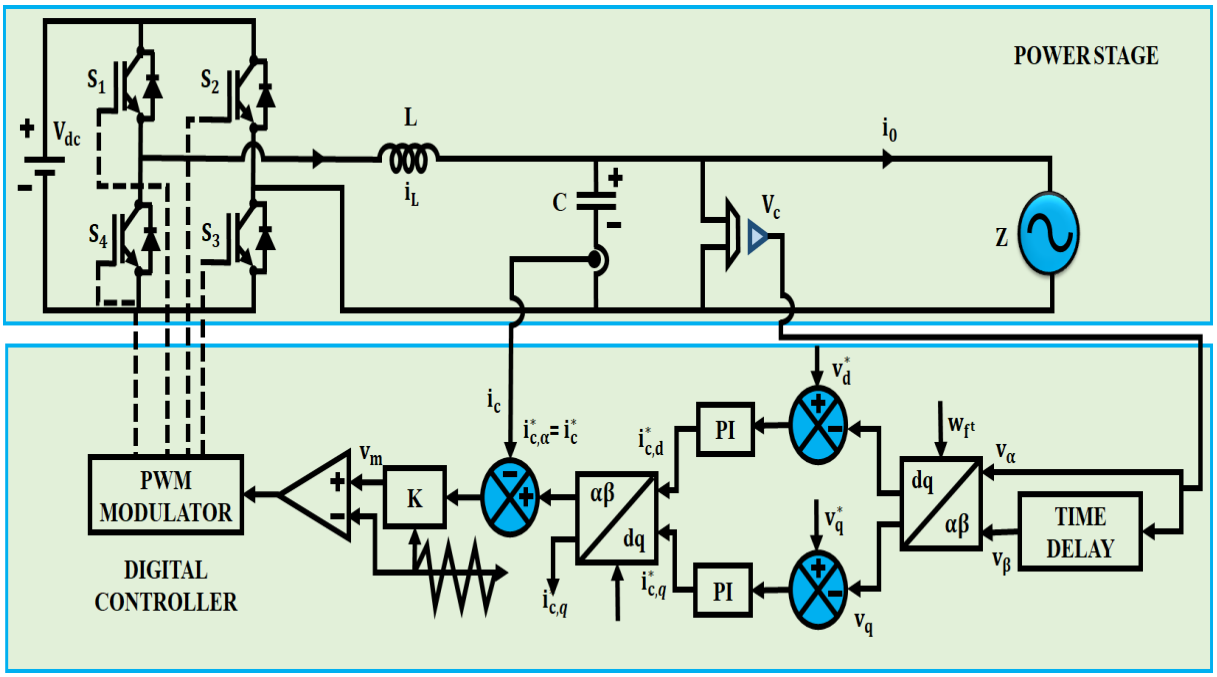

Figure 8. Dq theory based voltage control for 1φ VSI

By ensuring that the output voltage waveform of the VSI satisfies grid code standards, this procedure avoids problems with over voltage. The system employs a voltage feedback control approach for the single phase VSI and adds an additional filter capacitor current. Park's transformation is used, as shown in Figure. 8, with the electric signal from the time delay block serving as the βaxis (v_β) input and the filter capacitor voltage (v_c) serving as the α-axis (v_α) input. Accurate phase alignment and efficient voltage management are ensured by this arrangement.

The filter capacitor voltage (v_c) is referenced in the stationary frame by the signal$v_c^* = V_{Cm}cos(w_f t)$. As a result, the time delay block causes a one-quarter delay of (T_f) in the time domain. By doing this, (v_c) is guaranteed to be orthogonal to (v_β). Furthermore, the q and d axis voltage magnitudes are set to particular reference values, where ($v_q^* = 0$) and ($v_d^* = V_{Cm}$), respectively. A Proportional Integral (PI) controller is exploited to adjust for any variations in (v_d) and (v_q). Inverse Park's transformation is then exploited to transform the electrical signals back to the stationary reference frame. The filter capacitor current (v_c) is represented by the α-axis output in the current control loop.

The proportional controller adjusts any deviations in the filter capacitor current to maintain the desired current level. In the end, this procedure produces the modulation signal (v_m), which is essential for regulating the output of the inverter. By sustaining constant voltage and current outputs even in the face of fluctuating load and input conditions, the modulation signal guarantees effective inverter functioning.

4. Result and Discussion

An MPPT controller based ANFIS is developed in this study for an optimal renewable energy integration system for PV. The MATLAB platform simulations for this work and results are shown below.

Table 1. Parameter specification

Parameter	Specification
PV System	
Rated Power	10*kW*
No. of panels in Parallel	15
Open circuit Voltage	37.25*V*
Cell linked in Series	36
No. of Panels in series	3
Short Circuit Current	8.95 *A*
Modified Luo Converter	
L_1, L_2, L_3	4.7 *mH*
Switching frequency	10*KHz*
C_1, C_2, C_3	22*μF*

Case 1: PV System Performance under Steady State Condition

Figure. 9 shows the PV panel's continuous working conditions. The panel's temperature waveform, which stays constant at 35°C, is displayed in Fig. 9a. Fig 9b represents the intensity waveform, with a steady value of 1000 W/m². Fig 9c displays the voltage waveform, which maintains a consistent value of 110 V. Fig 9d shows the output waveform, a sinusoidal current of 37A. All three parameters remain unchanged over time, depicting the stable operating environment of the PV panel.

Figure 10 depicts the waveforms of the Modified Luo Converter. Fig 10a illustrates the input current waveform, which remains constant at 320V. Figure 10b presents a steady current waveform of 10A. These waveforms demonstrate the consistent performance of the converter.

Figure 11 represent modified luo converter power waveform, Fig 11a shows the input power waveform of the modified Luo converter, which increases to 3200W and remains constant. Figure 11b illustrates the output power waveform, which increases to 3500W and follows a sinusoidal path. These waveforms depict the power characteristics of modified Luo converter under operation.

Case 2: PV System Performance under Varying Temperature and Intensity

PV's stable working conditions are shown in Figure. 12. The panel's temperature waveform, which stays constant at 36°C, is displayed in Figure. 12a. the intensity waveform, with a constant value of 1000W/m2, is shown in Figure. 12b. Figure 12c presents voltage waveform, which consistently holds at 120V. Fig 12d shows the input current, which rises rapidly to 40 A and exhibits oscillations around 0.2 and 0.3 seconds before stabilizing. Together, these parameters remain unchanged over time, highlighting the stable operating environment of the PV panel.

Figure 13 illustrates performance of developed converter waveforms. Figure 13a depicts the output voltage regulated by an ANFIS MPPT controller, stabilizing at 350 to 400 V with minor transients at the same intervals. Fig 13b represents the output current, which smoothly reaches 10 A, with slight oscillations at 0.2 and 0.3 seconds. These waveforms highlight the converter's stability and the effectiveness of the ANFIS controller in managing transient conditions.

Figure 14 shows the power waveforms of a modified Luo converter. Fig 14a depicts the input power rising to 3500 W with transient disturbances at 0.2 and 0.3 seconds.

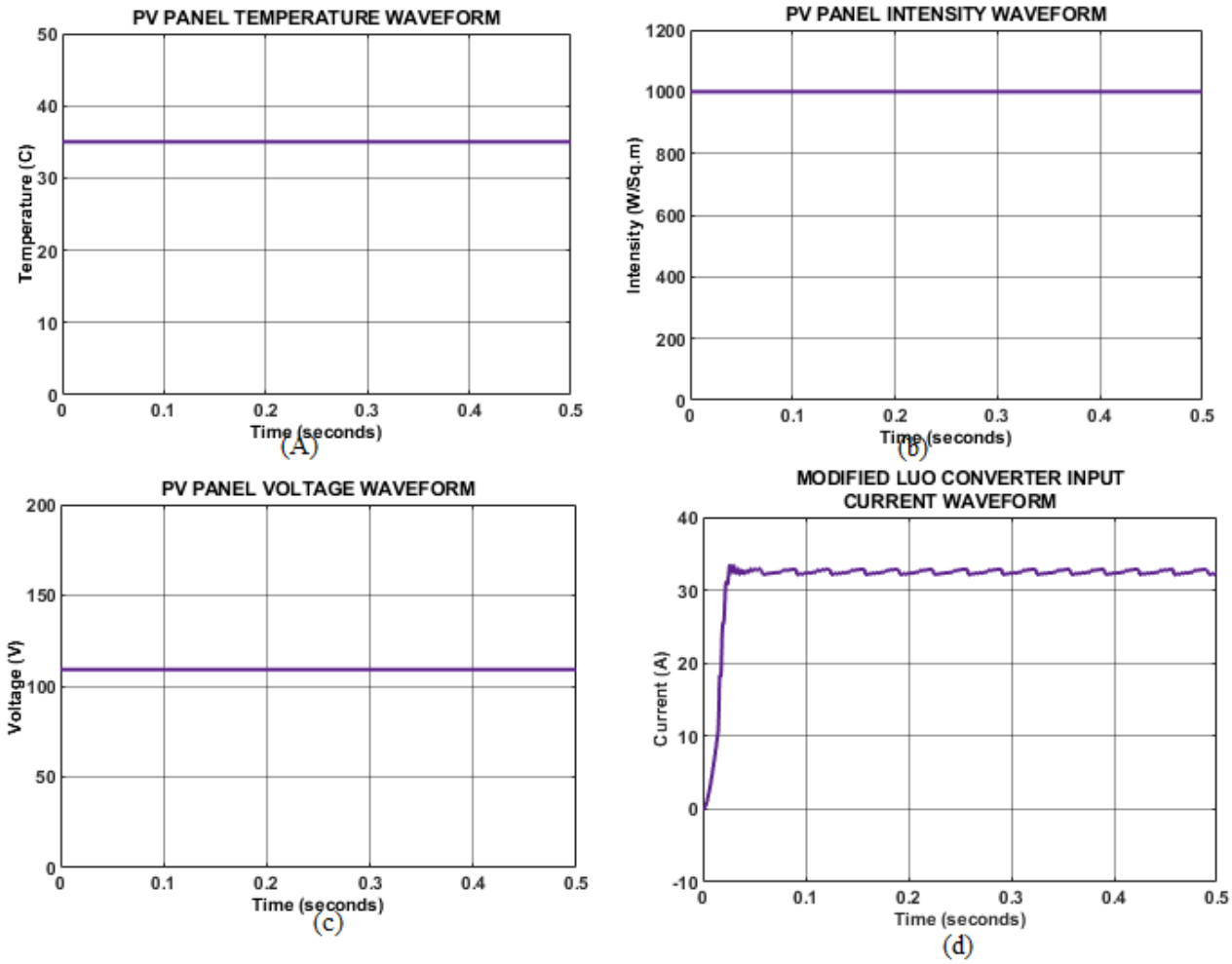

Figure 9. Operating Conditions of the PV Panel

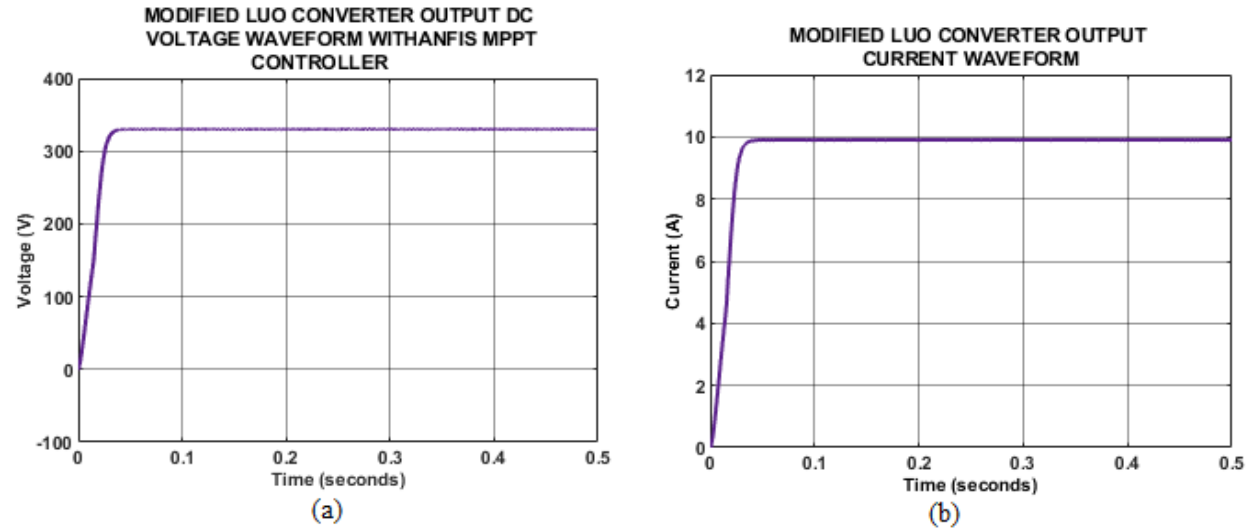

Figure 10. Modified Luo Converter waveform

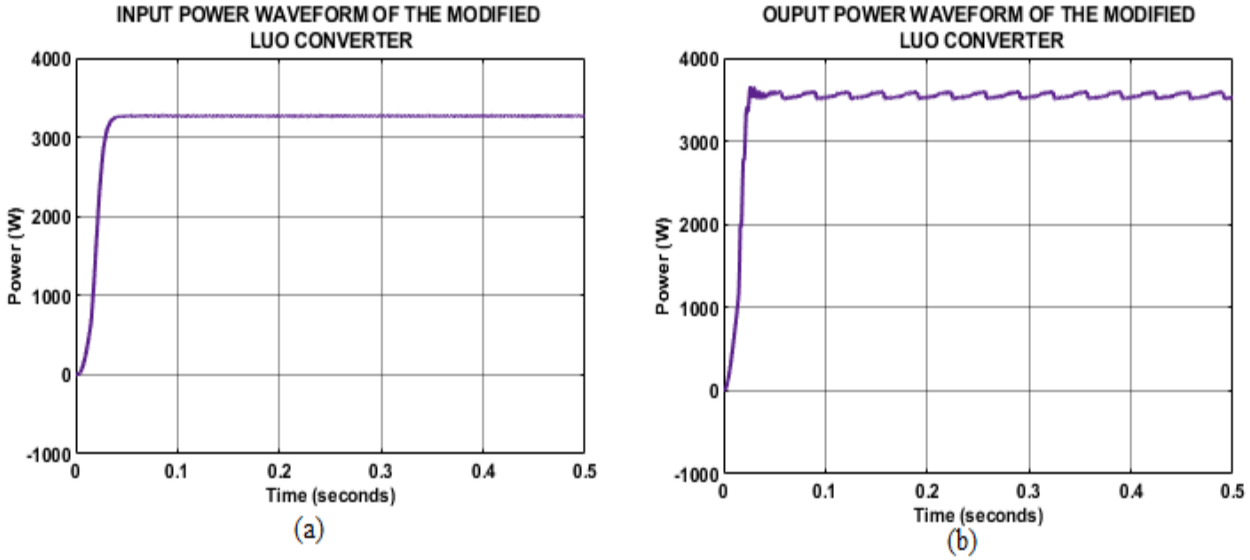

Figure 11. Power Waveforms of the Modified Luo Converter

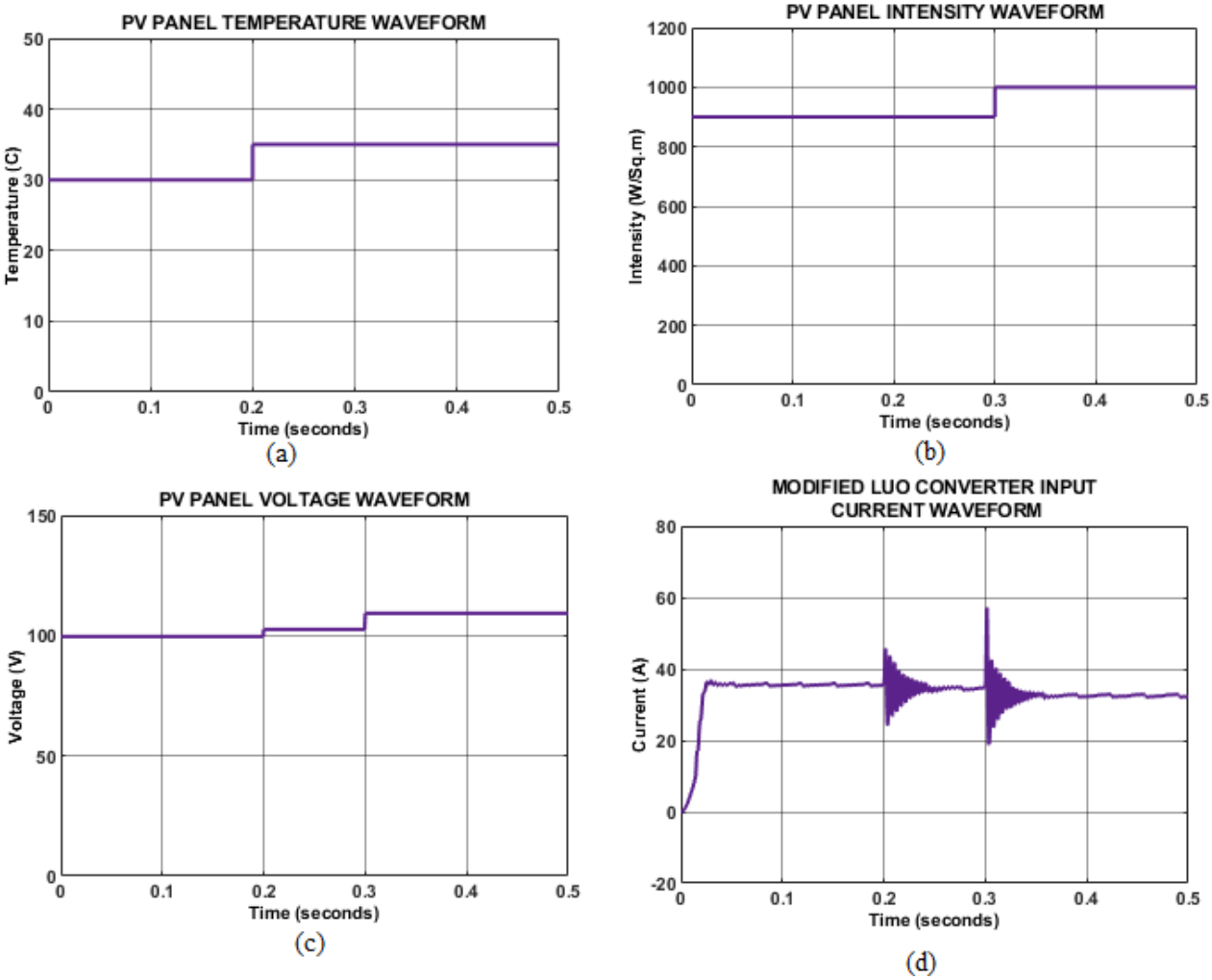

Figure 12. Three waveform of PV panel

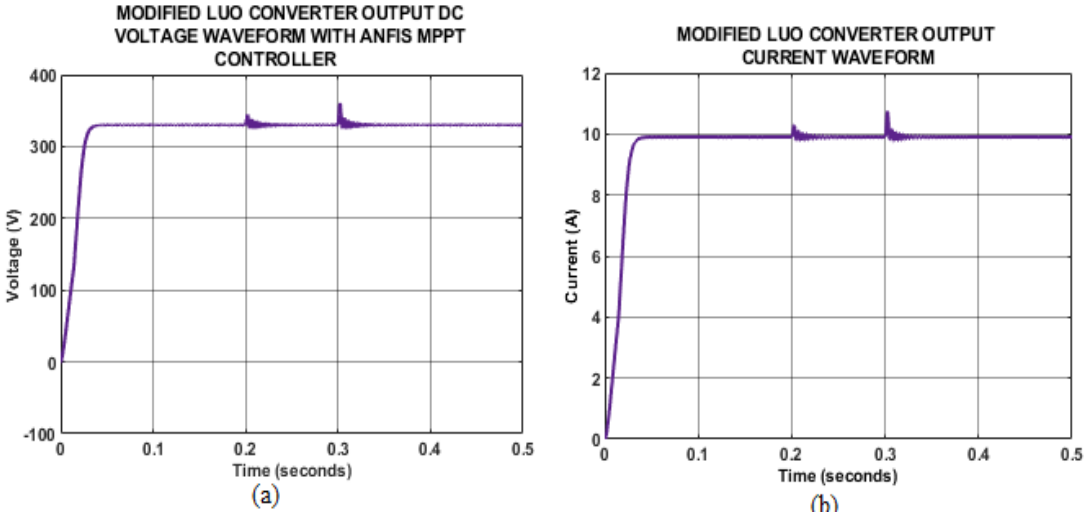

Figure 13. Three waveform of modified Luo converter

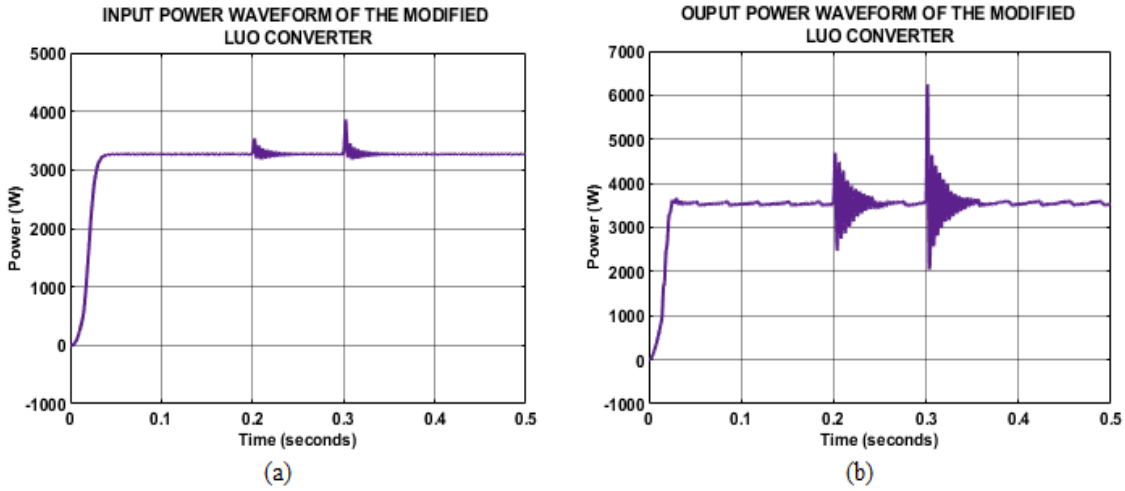

Figure 14. Waveform of power and modified Luo converter

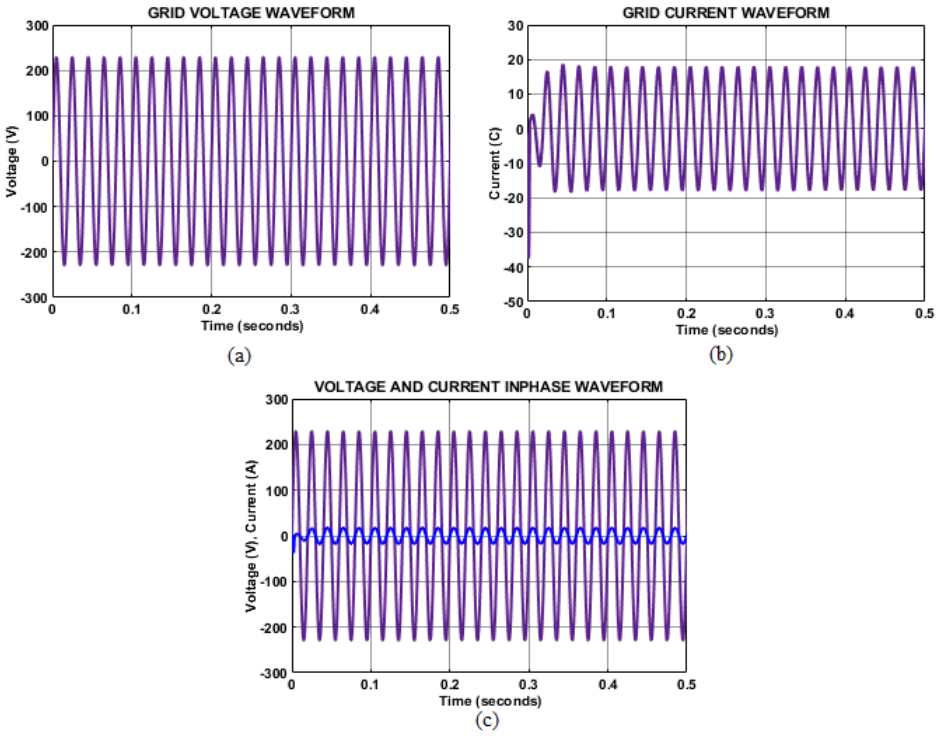

Figure 15. Grid voltage and current waveform

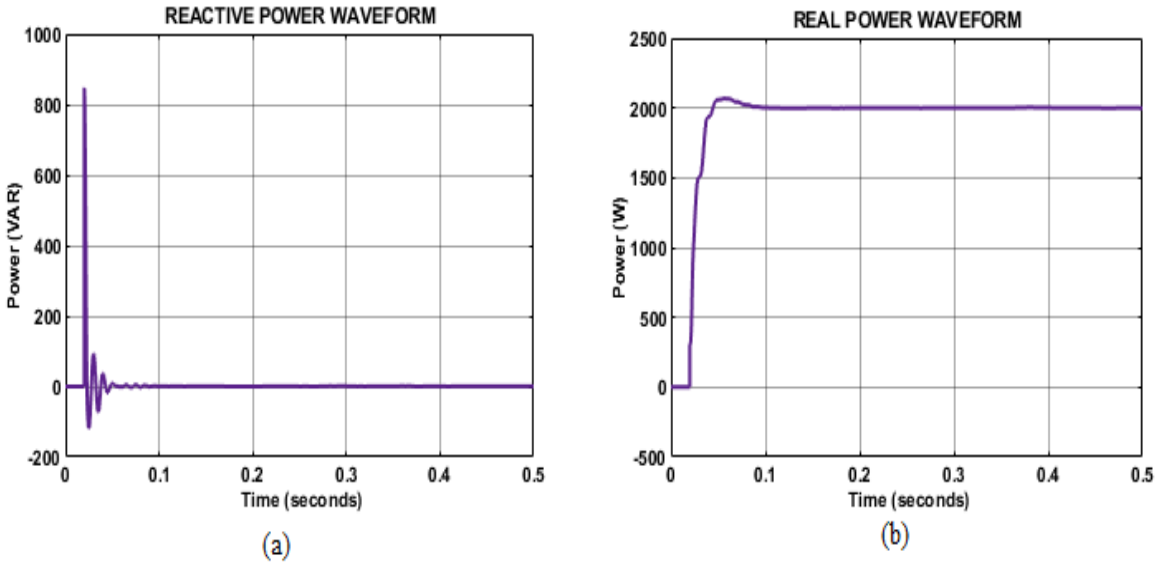

Figure 16. Waveform of reactive and real power waveform

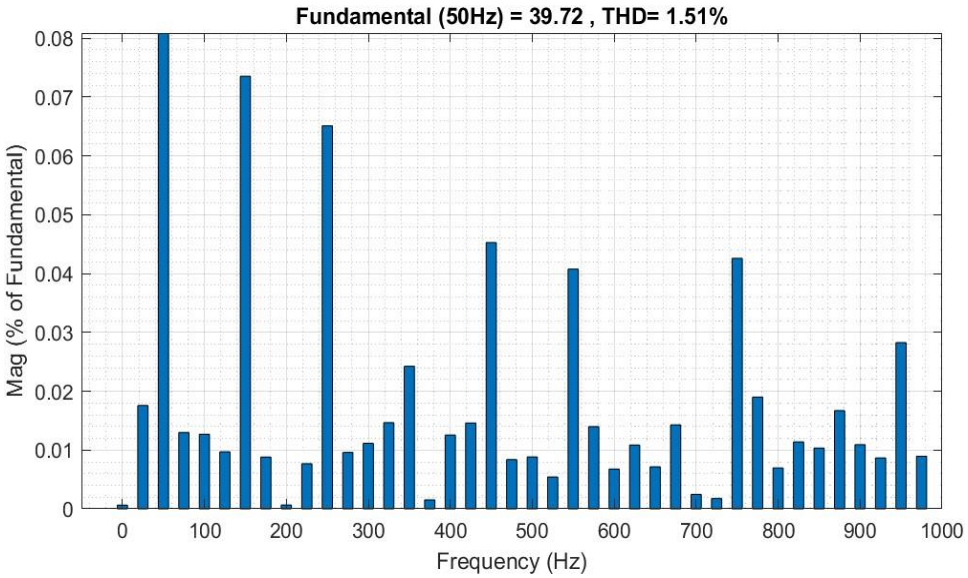

Figure 17. THD values

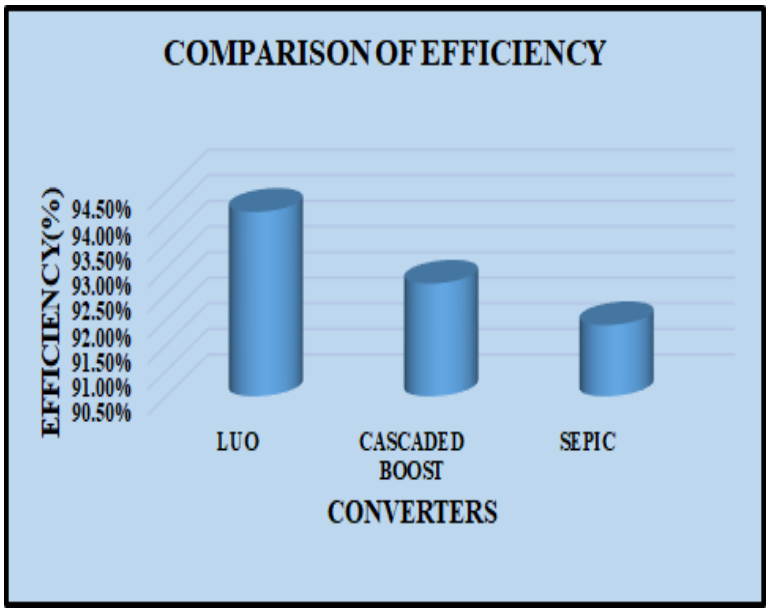

Figure 18. Comparison of efficiency

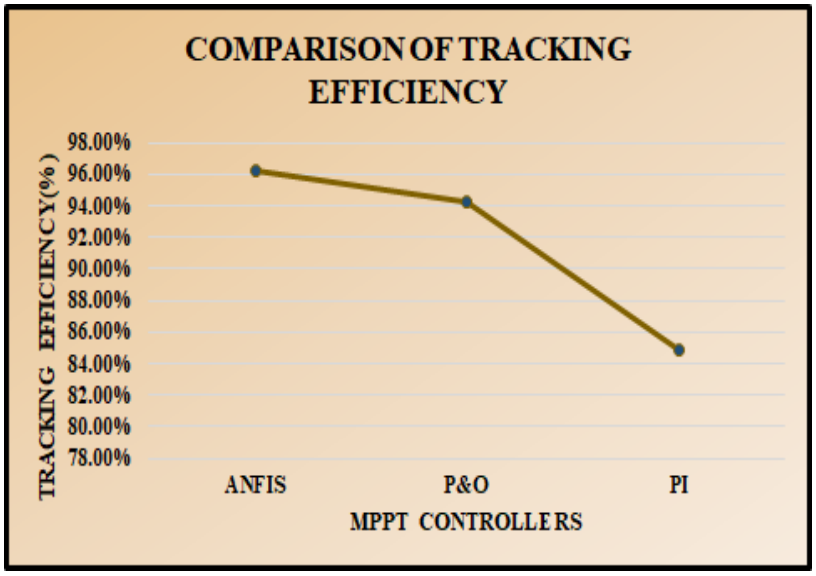

Figure 19. Comparison of tracking efficiency

Figure 14b shows the output power reaching 3000 to 4000W, with significant oscillations at same intervals. Both waveforms demonstrate stable performance with brief transient effects.

Figure 14 illustrates the grid voltage and current waveforms, highlighting their sinusoidal and in phase characteristics. Figure 15a shows the grid voltage oscillating smoothly between ±300 V over 0.5 seconds, maintaining a consistent sinusoidal pattern. Figure 15b depicts the grid current following a similar sinusoidal waveform, oscillating between ±30 A with steady behavior. Figure 15c combines the voltage and current waveforms, showing that they are in phase, which indicates efficient power transfer with minimal reactive power. These waveforms highlight the stable and synchronized operation of the grid current and voltage.

Figure 16 illustrates the waveforms of reactive and real power. In Figure 16a, the reactive power waveform (in VAR) remains stable, indicating consistent reactive power management within the system. Similarly, Figure 16b depicts the real power waveform, which stays constant at 2000 W. This steady real power demonstrates reliable energy delivery, ensuring dependable system operation.

Figure 17 presents the THD values of the grid system, highlighting variations in harmonic distortion. The overall THD value is 1.51%, demonstrating that the system operates within acceptable harmonic distortion limits, ensuring efficient and stable performance.

Figure 18 compares the efficiency of various converters, highlighting the proposed Modified Luo converter achieves highest efficiency of 94.1%, denoting its better energy conversion ability than other approaches. Then, the Cascaded Boost converter [17] has an efficacy of 92.7%, indicating a better performance but lesser than developed converter. Meanwhile, the SEPIC converter [18] has the very lowest efficacy of 91.89 %, represents higher losses. The LUO converter outperforms the other two converters in terms of minimizing energy loss, making it potentially more appropriate for applications necessitating high efficacy.

Figure 19 compares the tracking efficiency of various MPPT controllers, showing that the proposed ANFIS controller achieves the highest efficiency at 96.23%. The P&O approach [19] has a slightly lower efficiency of 94.26 %, signifying moderate efficacy but with some limitations in dynamic response compared to ANFIS. The PI controller [20] exhibits the lowest tracking efficiency of 84.91%, replicating slower response and less optimal performance in quickly varying conditions. This comparison clearly highlights the benefit of intelligent control approaches like ANFIS in maximizing the power output of PV systems.

5. Conclusion

The proposed grid tied PV system integrating a Modified Luo Converter and an ANFIS based MPPT technique, demonstrates a robust and efficient solution for renewable energy integration. The Modified Luo Converter ensures stable DC-DC conversion under varying environmental conditions, while the ANFIS MPPT controller achieves accurate and reliable energy extraction by dynamically tracking the maximum power point of the PV array. Additionally, the single phase VSI is equipped with PI controller and synchronized pulse width modulation strategies, ensures seamless and high quality power delivery to the grid, complying with grid standards. Results of simulations using MATLAB 2021a Simulink validate superior performance of system, achieving an efficiency of 94.1% and contributing to enhanced grid stability. The capability of the developed approach to satisfy the growing need for effective, sustainable renewable energy is demonstrated in this research, which improves grid-connected PV system topologies.

References

[1] M. Badoni, A. Singh, A. K. Singh, H. Saxena, R. Kumar, Grid tied solar PV system with power quality enhancement using adaptive generalized maximum Versoria criterion. CSEE Journal of Power and Energy Systems, 9(2), (2021) 722–732.

[2] M.H. Ibrahim, S.P. Ang, M.N. Dani, M.I. Rahman, R. Petra, S.M. Sulthan, Optimizing step-size of perturb & observe and incremental conductance MPPT techniques using PSO for grid-tied PV system. IEEE access, 11, (2023) 13079–13090. https://doi.org/10.1109/ACCESS.2023.3242979

[3] H. Aloufi, R. Abbassi, B. Alhamazani, A. Albaker, M. Alturki, S. Albadran, Control and performance analysis of a grid-tied solar PV system International Journal of Advanced and Applied Sciences, 9(10), (2022) 1–10. https://orcid.org/0000-0001-8257-6721

[4] F. Wu, B. Yang, A. Hu, Y. Zhang, W. Ge, L. Ni, C. Wang, Y. Zha, Inertia and damping analysis of grid-tied photovoltaic power generation system with DC voltage droop control. IEEE Access, 9, (2021) 38411–38418. https://doi.org/10.1109/ACCESS.2021.3059687

[5] A.I.M. Ali, H.H.H. Mousa, H.R.A. Mohamed, S. Kamel, A.S. Hassan, Z.M. Alaas, E. E.M. Mohamed, A.R. Abdallah, An enhanced P&O MPPT algorithm with concise search area for grid-tied PV systems. IEEE Access, 11, (2023) 79408–79421. https://doi.org/10.1109/ACCESS.2023.3298106

[6] Y. León-Ruiz, M. González-García, R. Alvarez-Salas, J. Cuevas-Tello, V. Cárdenas, Fault diagnosis based on machine learning for the high frequency link of a grid-tied photovoltaic converter for a wide range of irradiance conditions. IEEE Access, 9, (2021) 151209–151220. https://doi.org/10.1109/ACCESS.2021.3126706

[7] A.S. Saidi, Impact of grid-tied photovoltaic systems on voltage stability of tunisian distribution networks using dynamic reactive power control. Ain Shams Engineering Journal, 13(2), (2022) 101537. https://doi.org/10.1016/j.asej.2021.06.023

[8] S.R. Kiran, C.H.H. Basha, V.P. Singh, C. Dhanamjayulu, B.R. Prusty, B. Khan, "Reduced simulative performance analysis of variable step size ANN based MPPT techniques for partially shaded solar PV systems. IEEE access, 10, (2022) 48875–48889. https://doi.org/10.1109/ACCESS.2022.3172322

[9] A.A.E. Tawfiq, M.O.A. El-Raouf, M.I. Mosaad, A.F.A. Gawad, M.A.E. Farahat, Optimal reliability study of grid-connected PV systems using evolutionary computing techniques. IEEE Access, 9, (2021) 42125–42139. https://doi.org/10.1109/ACCESS.2021.3064906

[10] D. Thivya Prasad, R. Anandhakumar, P. Balamurugan, Intelligent MPPT control for SEPIC-Luo converter in grid tied photovoltaic system. International Journal of Applied Power Engineering (IJAPE), 13(1), (20241) 102–112. http://doi.org/10.11591/ijape.v13.i1.pp102-112

[11] M. Bakkar, A. Aboelhassan, M. Abdelgeliel, M. Galea, PV systems control using fuzzy logic controller employing dynamic safety margin under normal and partial shading conditions. Energies, 14(4), (2021) 841. https://doi.org/10.3390/en14040841

[12] T. Rajesh, B. Gunapriya, M. Sabarimuthu, S. Karthikkumar, R. Raja, M. Karthik. Frequency control of PV-connected micro grid system using fuzzy logic controller. Materials Today: Proceedings, 45, (2021) 2260-2264. https://doi.org/10.1016/j.matpr.2020.10.255

[13] D. Thivya Prasad, R. Anandha Kumar, P. Balamurugan, Enhancing Grid-Connected Solar Photovoltaic Systems with High Gain Interleaved Sepic-Luo Converter and Optimized Anfis-Based MPPT. ARPN Journal of Engineering and Applied Sciences, 19(11), (2024) 684–696. https://doi.org/10.59018/062490

[14] A. Jaiswal, P. Chandrawanshi, N. Gupta, G. Khatarkar, M. Murali, Grid Tied Electric Vehicle Charging Station by Bidirectional PV Based High Gain Integrated DC-DC Converter. International Journal of Advanced Trends in Engineering and Management (IJATEM), 3(3), (2024) 01–12. https://doi.org/10.59544/JCKD2617/IJATEMV03I03P1

[15] M. Nivedha, PV Connected Grid System Using Modified Boost Converter with AI Based Controller. International Journal of Advanced Trends in Engineering and Management (IJATEM), 3(5), (2024) 44–57. https://doi.org/10.59544/WWVI4457/IJATEMV03I05P4

[16] R.S. Preethishri, J. Anitha Roseline, K. Murugesan, M. Senthil Kumaran, Optimized power factor correction for high speed switched reluctance motor. Intelligent Automation & Soft Computing, 35, (2023) 997–1014. https://doi.org/10.32604/iasc.2023.025510

[17] H. Gholizadeh, R. Sharifi Shahrivar, M.R. Hashemi, E. Afjei, S.A. Gorji, Design and implementation a single-switch step-up DC-DC converter based on cascaded boost and luo converters. Energies, 14(12), (2021) 3584. https://doi.org/10.3390/en14123584

[18] D. Sibtain, M.M. Gulzar, K. Shahid, I. Javed, S. Murawwat, M. M. Hussain, Stability analysis and design of variable step-size P&O algorithm based on fuzzy robust tracking of MPPT for standalone/grid connected power system. Sustainability, 14(15), (2022) 8986.

https://doi.org/10.3390/su14158986

[19] C.P. Mutharasan Anburaj, Fatigue mitigation of wind turbine system using multiple point model predictive control. International Journal of Power Electronics and Drive Systems (IJPEDS), 12(4), (2021) 2261–2272. http://doi.org/10.11591/ijpeds.v12.i4.pp2261-2272

[20] D. Verma, S. Nema, A.M. Shandilya, and S.K. Dash, Maximum power point tracking (MPPT) techniques: Recapitulation in solar photovoltaic systems. Renewable and Sustainable Energy Reviews, 54 (2016)1018-1034. https://doi.org/10.1016/j.rser.2015.10.068

Authors Contribution Statement

D. Thivya Prasad: Conceptualization, Data Curation, Writing - Original Draft, Methodology, Project administration. R. Anandhakumar: Methodology, Project administration, Supervision. P. Balamurugan: Methodology, Project administration, Supervision. All authors read and approved the final version for submission.

Funding

The authors declare that no funds, grants or any other support were received during the preparation of this manuscript.

Competing Interests

The authors declare that there are no conflicts of interest regarding the publication of this manuscript.

Data Availability

The data supporting the findings of this study can be obtained from the corresponding author upon reasonable request.

Has this article screened for similarity?

Yes

About the License